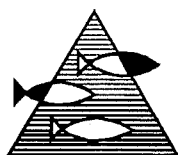


PROSJEKTRAPPORT



ISSN 0071-5638

HAVFORSKNINGSINSTITUTTET

MILJØ - RESSURS - HAVBRUK

Nordnesgt. 50 Postboks 1870 5024 Bergen

Tlf.: 55 23 85 00 Fax: 55 23 85 31

Forskningsstasjonen

Flødevigen

4817 His

Tlf.: 37 01 05 80

Fax: 37 01 05 15

Austevoll

Havbruksstasjon

5392 Storebø

Tlf.: 56 18 03 42

Fax: 56 18 03 98

Matre

Havbruksstasjon

5198 Matredal

Tlf.: 56 36 60 40

Fax: 56 36 61 43

Distribusjon:

ÅPEN

HI-prosjektnr.:

9210.1

Oppdragsgiver(e):

Oppdragsgivers referanse:

Rapport:

FISKEN OG HAVET

NR.12 - 1996

Tittel:

DESCRIPTION OF A SIGMA-COORDINATE
OCEAN MODEL

Senter:

Miljø

Seksjon:

Havmiljødata og modellering

Forfatter(e):

Jarle Berntsen, Morten D. Skogen og Terje O. Espelid

Antall sider, vedlegg inkl.:

35

Dato:

28.05.96

Sammendrag:

De siste årene har en havmodell basert på Blumberg og Mellors ECOM3D blitt benyttet ved Havforskningsinstituttet. Dette er en populær modell som blir benyttet ved en rekke institusjoner både nasjonalt og internasjonalt. Basert på de erfaringene en har gjort er det imidlertid mulig å peke på flere svakheter ved modellen. Med dette som utgangspunkt har men i et samarbeid mellom Universitetet i Bergen og Havforskningsinstituttet arbeidet for å utvikle en ny og bedre havmodell. I den nye modellen har man beholdt det beste av ECOM3D, samtidig som flere av de mindre gode delene er blitt erstattet. Denne rapporten er en dokumentasjon av versjon 1 av modellen.

Emneord - norsk:

1. Havmodell

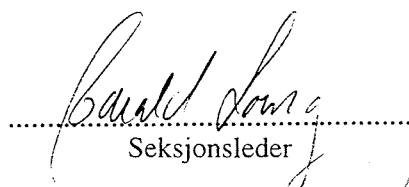
2. Brukerdokumentasjon

Emneord - engelsk:

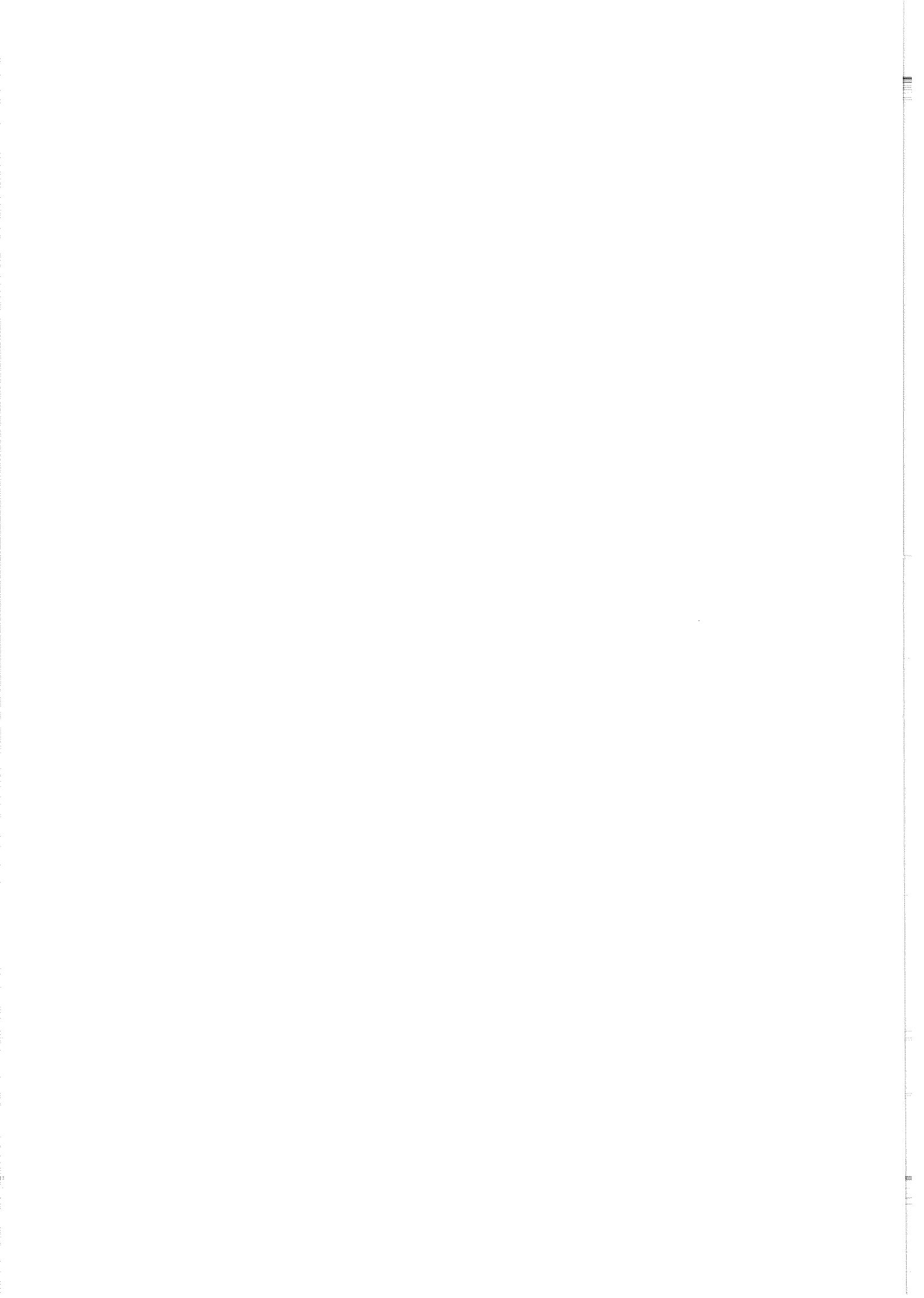
1. Ocean model

2. Ocean guide


.....
Prosjektleder


.....
Seksjonsleder

R 4571



Description of a σ -coordinate ocean model

Jarle Berntsen
Department of Mathematics Institute of Marine Research
University of Bergen Nordnesparken 2
Johs. Bruns gt. 12 N-5024 Bergen-Nordnes
N-5008 Bergen,

Morten Dahlberg Skogen
Institute of Marine Research
Nordnesparken 2
N-5024 Bergen-Nordnes
and

Terje O. Espelid
Department of Informatics
University of Bergen
Thormøhlens gt. 12
N-5008 Bergen

Contents

1	Introduction	1
2	The σ-coordinate model	2
2.1	The Basic Variables and Equations	2
2.1.1	Boundary conditions	4
2.2	The σ -coordinate system	5
2.2.1	Vertical boundary conditions	6
2.3	The numerical σ -coordinate model	7
2.4	Effects of the earths rotation	8
2.5	Surface gravity waves	8
2.6	The internal pressure	11
2.7	The atmospheric pressure	13
2.8	Advection	13
2.9	Subgrid scale vertical mixing processes	14
2.10	Subgrid scale horizontal mixing processes	17
2.11	Time step constraints	18
3	Model validation	19
3.1	Model validation using SKAGEX-90 data	19
3.2	Validation using an idealized test case	23
A	List of symbols	26
B	FORTRAN 90 variables	27
C	FORTRAN 90 subroutines	30

1 Introduction

This report is a documentation of a σ -coordinate numerical ocean model developed at the Institute of Marine Research and the University of Bergen. The work on the model started in 1995, and is expected to continue in the years to come.

Since the early 1990s a σ -coordinate model due to Blumberg and Mellor [6] has been used by the Norwegian ocean modeling community in a number of oceanographic studies [1, 4, 13, 21, 22, 23, 25]. This model performed successfully in a model validation, MOMOP [20], financed by Norwegian oil companies. The availability and use of this model has been of great importance to the applied oceanographic community in Norway both as a tool for studying important oceanographic problems, but also because a number of persons involved in this work gained better insight in the properties of the model.

Based on this insight and on knowledge about more recent numerical techniques, we believed that it would be possible to develop a σ -coordinate model that could produce in some sense more accurate model results. Techniques for ocean model validation that the user community can agree on have not yet been established, and thus it will be hard to state that one model is generally better than another. Nevertheless, we have proposed some tools for intercomparison of model data and measurements [5]. In this report observations from the SKAGEX experiment [7] are used to validate the models.

In section 2 the σ -coordinate model is described and in section 3 some results from experiments with the model are presented.

The model implemented on an idealized test case is available on request to one of the authors.

2 The σ -coordinate model

2.1 The Basic Variables and Equations

The symbols used in the description of the model are given in Appendix A. The model assumes that the weight of the fluid identically balances the pressure (hydrostatic assumption), and that density differences are neglected unless the differences are multiplied by gravity (Boussinesq approximation). The following equations are used to describe the variables as functions of the cartesian coordinates x, y, z .

The continuity equation is

$$\nabla \cdot \vec{U} + \frac{\partial W}{\partial z} = 0, \quad (1)$$

and the Reynolds momentum equations are

$$\frac{\partial U}{\partial t} + \vec{U} \cdot \nabla U + W \frac{\partial U}{\partial z} - fV = -\frac{1}{\rho_0} \frac{\partial P}{\partial x} + \frac{\partial}{\partial z} (K_M \frac{\partial U}{\partial z}) + F_x, \quad (2)$$

$$\frac{\partial V}{\partial t} + \vec{U} \cdot \nabla V + W \frac{\partial V}{\partial z} + fU = -\frac{1}{\rho_0} \frac{\partial P}{\partial y} + \frac{\partial}{\partial z} (K_M \frac{\partial V}{\partial z}) + F_y, \quad (3)$$

$$\rho g = -\frac{\partial P}{\partial z}. \quad (4)$$

The pressure at depth z may be obtained by integrating equation (4) vertically

$$P = P_{atm} + g\rho_0\eta + g \int_z^0 \rho(z') dz'. \quad (5)$$

The conservation equations for temperature and salinity are

$$\frac{\partial T}{\partial t} + \vec{U} \cdot \nabla T + W \frac{\partial T}{\partial z} = \frac{\partial}{\partial z} (K_H \frac{\partial T}{\partial z}) + F_T, \quad (6)$$

$$\frac{\partial S}{\partial t} + \vec{U} \cdot \nabla S + W \frac{\partial S}{\partial z} = \frac{\partial}{\partial z} (K_H \frac{\partial S}{\partial z}) + F_S. \quad (7)$$

The density is computed according to an equation of state of the form

$$\rho = \rho(T, S) \quad (8)$$

taken from [31].

Motions induced by small scale processes (sub-grid scale) are parameterized by horizontal and vertical eddy viscosity/diffusivity terms. The horizontal terms F_x , F_y , F_T and F_S may be written

$$F_x = \frac{\partial}{\partial x}(2A_M \frac{\partial U}{\partial x}) + \frac{\partial}{\partial y}(A_M(\frac{\partial U}{\partial y} + \frac{\partial V}{\partial x})), \quad (9)$$

$$F_y = \frac{\partial}{\partial y}(2A_M \frac{\partial V}{\partial y}) + \frac{\partial}{\partial x}(A_M(\frac{\partial U}{\partial y} + \frac{\partial V}{\partial x})), \quad (10)$$

$$F_{T,S} = \frac{\partial}{\partial x}(A_H \frac{\partial(T,S)}{\partial x}) + \frac{\partial}{\partial y}(A_H \frac{\partial(T,S)}{\partial y}). \quad (11)$$

The horizontal diffusivities, A_M and A_H , are computed according to Smagorinsky [26]

$$(A_M, A_H) = (C_M, C_H)\Delta x \Delta y \frac{1}{2}[(\frac{\partial U}{\partial x})^2 + \frac{1}{2}(\frac{\partial V}{\partial x} + \frac{\partial U}{\partial y})^2 + (\frac{\partial V}{\partial y})^2]^{\frac{1}{2}}. \quad (12)$$

2.1.1 Boundary conditions

At the free surface, $z = \eta(x, y)$, we have

$$\rho_0 K_M \left(\frac{\partial U}{\partial z}, \frac{\partial V}{\partial z} \right) = (\tau_{0x}, \tau_{0y}), \quad (13)$$

$$\rho_0 K_H \left(\frac{\partial T}{\partial z}, \frac{\partial S}{\partial z} \right) = (\dot{T}_0, \dot{S}_0). \quad (14)$$

There are no volume fluxes through the side walls. On the side walls and bottom of the basin there are no advective or diffusive heat and salt fluxes. The vertical velocities at the free surface and at the bottom are given by

$$W_0 = U \frac{\partial \eta}{\partial x} + V \frac{\partial \eta}{\partial y} + \frac{\partial \eta}{\partial t}, \quad (15)$$

$$W_b = -U_b \frac{\partial H}{\partial x} - V_b \frac{\partial H}{\partial y}. \quad (16)$$

The effect of the bottom drag on horizontal velocities is given by

$$\rho_0 K_M \left(\frac{\partial U}{\partial z}, \frac{\partial V}{\partial z} \right) = (\tau_{bx}, \tau_{by}). \quad (17)$$

$$(18)$$

The bottom stress is specified by

$$\vec{\tau}_b = \rho_0 C_D |\vec{U}_b| \vec{U}_b \quad (19)$$

where the drag coefficient C_D is given by

$$C_D = \max\left[0.0025, \frac{\kappa^2}{(\ln(z_b/z_0))^2}\right] \quad (20)$$

and z_b is the distance of the nearest grid point to the bottom. The von Karman constant $\kappa = 0.4$. In lack of further information we use $z_0 = 0.01m$ for the bottom roughness parameter, see Weatherly and Martin [33].

2.2 The σ -coordinate system

The basic equations have been transformed into a bottom following sigma coordinate system [19]. The independent variables (x, y, z, t) are transformed to (x^*, y^*, σ, t^*) , where

$$x^* = x \quad y^* = y \quad \sigma = \frac{z - \eta}{H + \eta} \quad t^* = t. \quad (21)$$

σ ranges from $\sigma = 0$ at $z = \eta$ to $\sigma = -1$ at $z = -H(x, y)$. Introducing the total depth, $D \equiv H + \eta$, the basic equations may now be written as (after deletion of the asterisks)

$$\frac{\partial UD}{\partial x} + \frac{\partial VD}{\partial y} + \frac{\partial \omega}{\partial \sigma} + \frac{\partial \eta}{\partial t} = 0 \quad (22)$$

where ω is the new vertical velocity. The momentum equations on flux form become

$$\begin{aligned} \frac{\partial UD}{\partial t} + \frac{\partial U^2 D}{\partial x} + \frac{\partial UV D}{\partial y} + \frac{\partial U \omega}{\partial \sigma} - fVD + \frac{D}{\rho_0} \frac{\partial P_{atm}}{\partial x} + gD \frac{\partial \eta}{\partial x} = \\ \frac{\partial}{\partial \sigma} \left(\frac{K_M}{D} \frac{\partial U}{\partial \sigma} \right) - \frac{gD^2}{\rho_0} \int_{\sigma}^0 \left(\frac{\partial \rho}{\partial x} - \frac{\sigma}{D} \frac{\partial D}{\partial x} \frac{\partial \rho}{\partial \sigma} \right) d\sigma + DF_x, \end{aligned} \quad (23)$$

$$\begin{aligned} \frac{\partial VD}{\partial t} + \frac{\partial UV D}{\partial x} + \frac{\partial V^2 D}{\partial y} + \frac{\partial V \omega}{\partial \sigma} + fUD + \frac{D}{\rho_0} \frac{\partial P_{atm}}{\partial y} + gD \frac{\partial \eta}{\partial y} = \\ \frac{\partial}{\partial \sigma} \left(\frac{K_M}{D} \frac{\partial V}{\partial \sigma} \right) - \frac{gD^2}{\rho_0} \int_{\sigma}^0 \left(\frac{\partial \rho}{\partial y} - \frac{\sigma}{D} \frac{\partial D}{\partial y} \frac{\partial \rho}{\partial \sigma} \right) d\sigma + DF_y. \end{aligned} \quad (24)$$

The new conservation equations take the form

$$\frac{\partial TD}{\partial t} + \frac{\partial TUD}{\partial x} + \frac{\partial TVD}{\partial y} + \frac{\partial T\omega}{\partial \sigma} = \frac{\partial}{\partial \sigma} \left(\frac{K_H}{D} \frac{\partial T}{\partial \sigma} \right) + DF_T, \quad (25)$$

$$\frac{\partial SD}{\partial t} + \frac{\partial SUD}{\partial x} + \frac{\partial SVD}{\partial y} + \frac{\partial S\omega}{\partial \sigma} = \frac{\partial}{\partial \sigma} \left(\frac{K_H}{D} \frac{\partial S}{\partial \sigma} \right) + DF_S, \quad (26)$$

and the horizontal viscosity and diffusion terms are now defined according to

$$DF_x = \frac{\partial}{\partial x} (2DA_M \frac{\partial U}{\partial x}) + \frac{\partial}{\partial y} (DA_M (\frac{\partial U}{\partial y} + \frac{\partial V}{\partial x})), \quad (27)$$

$$DF_y = \frac{\partial}{\partial y}(2DA_M \frac{\partial V}{\partial y}) + \frac{\partial}{\partial x}(DA_M(\frac{\partial U}{\partial y} + \frac{\partial V}{\partial x})), \quad (28)$$

$$DF_{T,S} = \frac{\partial}{\partial x}(DA_H \frac{\partial(T,S)}{\partial x}) + \frac{\partial}{\partial y}(DA_H \frac{\partial(T,S)}{\partial y}). \quad (29)$$

It should be noted that several terms originating from the σ -coordinate transformation are neglected in equations (27), (28) and (29). These simplified formulations for horizontal viscosity/diffusivity terms in σ -coordinate models are suggested by Mellor and Blumberg [14]. In [14] a description of the complete terms is also given.

2.2.1 Vertical boundary conditions

The new boundary conditions for the vertical velocity, ω , in equation (22) become

$$\omega(0) = \omega(-1) = 0. \quad (30)$$

The new conditions at the surface ($\sigma = 0$) becomes

$$\frac{K_M}{D} \left(\frac{\partial U}{\partial \sigma}, \frac{\partial V}{\partial \sigma} \right) = \frac{1}{\rho_0} (\tau_{0x}, \tau_{0y}), \quad (31)$$

$$\frac{K_H}{D} \left(\frac{\partial T}{\partial \sigma}, \frac{\partial S}{\partial \sigma} \right) = (\dot{T}_0, \dot{S}_0), \quad (32)$$

and at the bottom ($\sigma = -1$) the boundary conditions become

$$\frac{K_M}{D} \left(\frac{\partial U}{\partial \sigma}, \frac{\partial V}{\partial \sigma} \right) = \frac{1}{\rho_0} (\tau_{bx}, \tau_{by}), \quad (33)$$

$$\frac{K_H}{D} \left(\frac{\partial T}{\partial \sigma}, \frac{\partial S}{\partial \sigma} \right) = 0. \quad (34)$$

2.3 The numerical σ -coordinate model

The governing equations form a set of simultaneous partial differential equations which cannot be solved using known analytic methods. Therefore the equations have been discretized using finite difference methods. The horizontal finite difference scheme is staggered, and the Arakawa C-grid [17] has been used, see Figure 1.

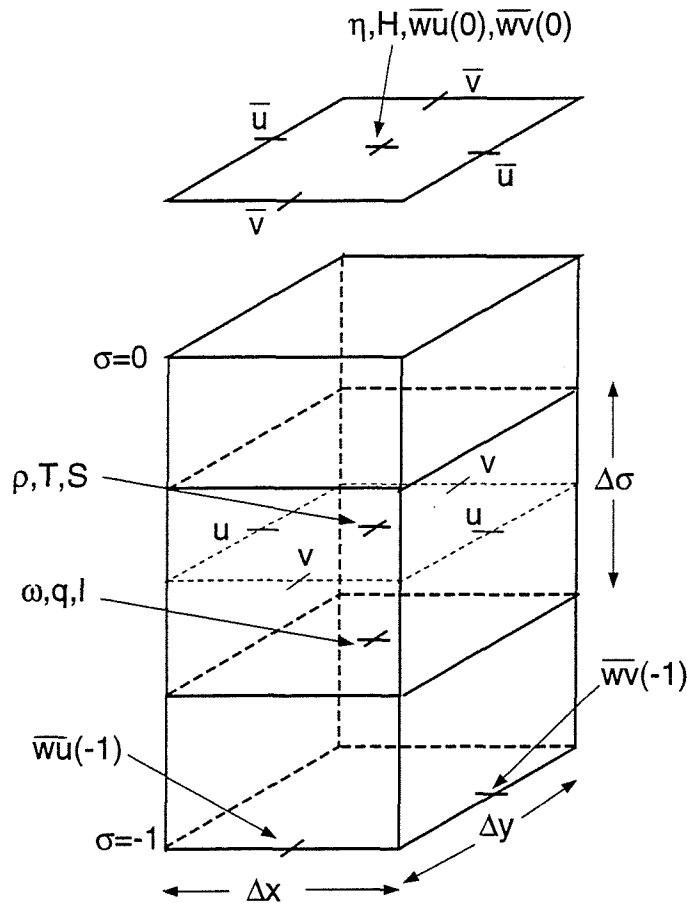


Figure 1. The location of variables in the C-grid

The model is written in FORTRAN 90 and the discrete versions of the state variables and parameters are gathered in a module, STATE, that may be addressed by all subroutines. Equations (22) - (26) are stepped forward in time using the same time step for all equations. The method of fractional steps is applied. That is a sequence of subroutines is called to perform specific subtasks and update the corresponding

variables in MODULE STATE in each timestep. After all subroutines are called the effects of all terms in the governing equations are included.

A description of the variables in MODULE STATE is given in Appendix B and an overview over the tasks of different subroutines is given in Appendix C. Descriptions of how different physical effects are included are given in the following sections.

When describing the finite difference approximations to the governing equations, the following sum and difference operators are used

$$\begin{aligned}\mu_x F(x, y, \sigma, t) &= (F(x + \Delta x/2, y, \sigma, t) + F(x - \Delta x/2, y, \sigma, t))/2 \\ \delta_x F(x, y, \sigma, t) &= (F(x + \Delta x/2, y, \sigma, t) - F(x - \Delta x/2, y, \sigma, t))/\Delta x \\ \mu_{xy} F(x, y, \sigma, t) &= (F(x + \Delta x/2, y + \Delta y/2, \sigma, t) + F(x + \Delta x/2, y - \Delta y/2, \sigma, t) + \\ &\quad F(x - \Delta x/2, y - \Delta y/2, \sigma, t) + F(x - \Delta x/2, y + \Delta y/2, \sigma, t))/4.\end{aligned}$$

2.4 Effects of the earths rotation

The subsystem of differential equations that describes the effects of the earths rotation may be written

$$\begin{aligned}\frac{\partial UD}{\partial t} &= fVD, \\ \frac{\partial VD}{\partial t} &= -fUD.\end{aligned}\tag{35}$$

This subsystem (35) is a coupled system of two ordinary differential equations which may be solved exactly if U and V were defined in the same points in space. The solutions for U and V at the new time step $n + 1$ are approximated by

$$U_{ijk}^{n+1} = \alpha U_{ijk}^n + \beta \mu_{xy} (V_{ijk}^n D_{Vij}^n) / D_{Uij}^n,\tag{36}$$

$$V_{ijk}^{n+1} = \alpha V_{ijk}^n - \beta \mu_{xy} (U_{ijk}^n D_{Uij}^n) / D_{Vij}^n.\tag{37}$$

where D_U and D_V are the dynamic depths $H + \eta$ in U -points and V -points respectively and $\alpha = \cos(f\Delta t)$, $\beta = \sin(f\Delta t)$. These operations are performed by the routine CORIOLIS.

2.5 Surface gravity waves

There is no time splitting in the model. This simplifies the structure of the code considerably. The fast surface gravity waves are treated with a spatially split implicit

time stepping technique. The use of an implicit scheme for the water elevation facilitates the use of the same time steps for all equations. The spatial splitting reduces the computational complexity and is described in [2].

The CFL-criterion imposed when applying explicit methods in free surface ocean circulation studies, very often forces us to apply smaller time step than necessary to resolve the major physical processes. When applying implicit methods, the CFL-criterion may be avoided or the bound on the time step increased. On the other hand linear systems of equations have to be solved at each time step, and the extra cost of using implicit methods may be significant.

A third approach is to split the system of differential equations in several subsystems of equations. By choosing appropriate numerical techniques for each subsystem the CFL-criterion is affected and may be removed. The cost of solving each subproblem and also the total cost is often only a small fraction of the cost of applying implicit methods to the complete system.

Subsystems of equations (23), (24) and the vertically integrated equation (22) may be written

$$\begin{aligned}\frac{\partial UD}{\partial t} &= -gD \frac{\partial \eta}{\partial x}, \\ \frac{\partial VD}{\partial t} &= -gD \frac{\partial \eta}{\partial y}, \\ \frac{\partial \eta}{\partial t} &= -\frac{\partial \bar{U}D}{\partial x} - \frac{\partial \bar{V}D}{\partial y},\end{aligned}\tag{38}$$

where $(\bar{U}, \bar{V}) = \int_{-1}^0 (U, V) d\sigma$. This system of differential equations may be split into the following two subsystems

$$\begin{aligned}\frac{\partial UD}{\partial t} &= -gD \frac{\partial \eta}{\partial x} \\ \frac{\partial VD}{\partial t} &= 0 \\ \frac{\partial \eta}{\partial t} &= -\frac{\partial \bar{U}D}{\partial x},\end{aligned}\tag{39}$$

$$\begin{aligned}
\frac{\partial UD}{\partial t} &= 0 \\
\frac{\partial VD}{\partial t} &= -gD \frac{\partial \eta}{\partial y} \\
\frac{\partial \eta}{\partial t} &= -\frac{\partial \bar{V}D}{\partial y}
\end{aligned} \tag{40}$$

Subsystems (39) and (40) are both one-dimensional, and may be propagated in time with the Crank-Nicholson method. Using (39) to update U and η we get

$$U_{ijk}^{n+1} = U_{ijk}^n - \frac{\Delta t}{2} g \delta_x (\eta_{ij}^{n+1} + \eta_{ij}^n) \tag{41}$$

$$\bar{U}_{ij}^n = \sum_{k=1}^{KB-1} U_{ijk}^n (DZ)_k \tag{42}$$

$$\eta_{ij}^{n+1} = \eta_{ij}^n - \Delta t \delta_x (\bar{U}_{ij}^n D_{Uij}^n) + \frac{(\Delta t)^2}{4} g \delta_x (D_{Uij}^n \delta_x (\eta_{ij}^{n+1} + \eta_{ij}^n)), \tag{43}$$

where DZ is the σ -coordinate layer thicknesses. These operations are performed by the routine SPLITGX. Using (40) to update V and η we get

$$V_{ijk}^{n+1} = V_{ijk}^n - \frac{\Delta t}{2} g \delta_y (\eta_{ij}^{n+1} + \eta_{ij}^n) \tag{44}$$

$$\bar{V}_{ij}^n = \sum_{k=1}^{KB-1} V_{ijk}^n (DZ)_k \tag{45}$$

$$\eta_{ij}^{n+1} = \eta_{ij}^n - \Delta t \delta_y (\bar{V}_{ij}^n D_{Vij}^n) + \frac{(\Delta t)^2}{4} g \delta_x (D_{Vij}^n \delta_y (\eta_{ij}^{n+1} + \eta_{ij}^n)). \tag{46}$$

These operations are performed by the routine SPLITGY. By numbering the grid cells in x -direction and y -direction respectively, the solution matrices for equations (43) and (46) become tridiagonal and are solved efficiently.

In the model the order of the operations are reversed every second step to make the operator symmetric. According to von Neumann analysis for free waves and constant depth this method is unconditionally stable.

It is known, Weare [32] and Stelling et al. [28], that due to the spatial splitting the shortest surface gravity modes are damped. In studies where tides are dominating and in studies where the free surface is in focus the use of spatial splitting techniques like the one described above should therefore be avoided. But in studies where the focus is on mean transports and on processes acting on a larger time scale, we have

found that it may have little or no effect on the quality of the results whether we apply the Crank-Nicolson method directly to the coupled system (38) or treat the two subsystems (39) and (40) separately, see Berntsen and Espelid [3]. On the other hand the splitting implies a substantial reduction in computational cost.

The Crank-Nicolson method applied to the coupled system (38) is implemented in the routine CRANK and an iterative solver for the corresponding system of equations is implemented in GAUSSIT. In the routine GAUSSIT there is a local parameter NUMIT (the number of iterations) that will depend on the given problem and the chosen time step.

Equation (22) with the surface boundary condition $\omega(0) = 0$ is used to compute ω at all layer interfaces. In all ocean cells ω_{ij1}^{n+1} is chosen to be zero and then (22) is integrated from the surface to the bottom by the algorithm

$$\begin{aligned} \omega_{ijk+1}^{n+1} = & \frac{\delta_x}{2} D_{ij}^n \sum_{K=1}^k (DZ)_K (U_{ijK}^{n+1} + U_{ijK}^n) + \\ & \frac{\delta_y}{2} D_{ij}^n \sum_{K=1}^k (DZ)_K (V_{ijK}^{n+1} + V_{ijK}^n) + \frac{\eta_{ij}^{n+1} - \eta_{ij}^n}{\Delta t} \sum_{K=1}^k (DZ)_K \end{aligned}$$

for $k = 1, KB-1$. Doing this, the bottom boundary condition $\omega(-1) = 0$ is satisfied to machine accuracy. The operations above are performed in the routine CRANK after the new values of the surface level and horizontal velocities are computed. When using spatial splitting, corresponding expressions are used to compute ω . The contributions to ω from the two substeps must then be added.

The routine WREAL computes the z -coordinate vertical velocities, WR, defined in S and T points from the equation

$$WR = \omega + U \left(\sigma \frac{\partial D}{\partial x} + \frac{\partial \eta}{\partial x} \right) + V \left(\sigma \frac{\partial D}{\partial y} + \frac{\partial \eta}{\partial y} \right) + (1 + \sigma) \frac{\partial \eta}{\partial t} \quad . \quad (47)$$

2.6 The internal pressure

The subsystem of equations (23) and (24) representing the internal pressure force in our σ -coordinate system is given by

$$\frac{\partial UD}{\partial t} = -\frac{gD^2}{\rho_0} \int_{\sigma}^0 \left(\frac{\partial \rho}{\partial x} - \frac{\sigma}{D} \frac{\partial D}{\partial x} \frac{\partial \rho}{\partial \sigma} \right) d\sigma, \quad (48)$$

$$\frac{\partial VD}{\partial t} = -\frac{gD^2}{\rho_0} \int_{\sigma}^0 \left(\frac{\partial \rho}{\partial y} - \frac{\sigma}{D} \frac{\partial D}{\partial y} \frac{\partial \rho}{\partial \sigma} \right) d\sigma. \quad (49)$$

This is a very important force which in areas with steep bottom topography, as we have in Norwegian waters, is difficult to approximate in σ -coordinate models. These problems are well documented, see for instance Haney [11]. On the other hand there are numerical evidence that despite the objections, finite difference approximations to the equations (48) and (49) give adequate representation of these forces in baroclinic studies, see Mellor et al. [15].

Stelling and van Kester [27] suggest to include the effect of internal pressure by treating these terms in z -coordinates

$$\frac{\partial U}{\partial t} = -\frac{g}{\rho_0} \frac{\partial}{\partial x} \int_z^0 \rho(\dot{z}) d\dot{z}, \quad (50)$$

$$\frac{\partial V}{\partial t} = -\frac{g}{\rho_0} \frac{\partial}{\partial y} \int_z^0 \rho(\dot{z}) d\dot{z}. \quad (51)$$

They choose a vertical integration technique that guarantees that in cases with no horizontal internal pressure gradients the corresponding numerical gradients also become zero. In a recent thesis work Slørdal [24] focus on the horizontal pressure gradient force in σ -coordinate ocean models in a number of diagnostic studies. He shows that the errors in velocities may be much larger when using the algorithm used in the Blumberg and Mellor model than the corresponding errors produced by the Stelling and van Kester algorithm. However, he finds that the Stelling and van Kester algorithm tend to underestimate the internal pressure force and thus give too small integrated transports.

In order to compute the gradients of equations (50) and (51) we need approximations to ρ at the depths of all U and V points of the σ -coordinate model. Slørdal suggest to use linear interpolation to get values ρ at required depths, and shows that this improves the accuracy of the integrated transports compared to the original Stelling and van Kester algorithm. Our findings from baroclinic studies support this conclusion, and the results also improve to some extent when using higher order splines in the vertical.

The finite difference approximations to equations (50) and (51) become

$$U_{ijk}^{n+1} = U_{ijk}^n - \frac{\Delta t g}{\rho_0} \delta_x \left(\frac{1}{2} (DZ)_1 D_{Uij} \rho_{ij1}^U + \sum_{k=1}^{k-1} \frac{1}{2} (DZ)_k D_{Uij} (\rho_{ijk}^U + \rho_{ijk+1}^U) \right), \quad (52)$$

$$V_{ijk}^{n+1} = V_{ijk}^n - \frac{\Delta t g}{\rho_0} \delta_y \left(\frac{1}{2} (DZ)_1 D_{Vij} \rho_{ij1}^V + \sum_{k=1}^{k-1} \frac{1}{2} (DZ)_k D_{Vij} (\rho_{ijk}^V + \rho_{ijk+1}^V) \right), \quad (53)$$

where all the variables at the right hands side are defined at time step n and the superscripts on ρ means that we have to approximate the densities at the depths of U and V points before applying the difference operators δ_x and δ_y . In the subroutine INTERNAL quadratic splines are used to perform the vertical interpolations. We have not found a clear improvement of the quality of the model results when using cubic splines that are computationally more expensive. The routine ZSPL2 is used to define the quadratic splines and SPL2 to perform the interpolations.

2.7 The atmospheric pressure

The third component of the pressure (5) is P_{atm} . Whenever this field is available, the subsystems of equations (23) and (24)

$$\frac{\partial UD}{\partial t} = -\frac{D}{\rho_0} \frac{\partial P_{atm}}{\partial x}, \quad (54)$$

$$\frac{\partial VD}{\partial t} = -\frac{D}{\rho_0} \frac{\partial P_{atm}}{\partial y} \quad (55)$$

are approximated by

$$U_{ijk}^{n+1} = U_{ijk}^n - \frac{\Delta t}{\rho_0} \delta_x P_{atm}^n, \quad (56)$$

$$V_{ijk}^{n+1} = V_{ijk}^n - \frac{\Delta t}{\rho_0} \delta_y P_{atm}^n. \quad (57)$$

These operations are performed by the routine ATMOSP.

2.8 Advection

The advective terms of equations (23), (24), (25) and (26) may all be written

$$\frac{\partial FD}{\partial t} + \frac{\partial FUD}{\partial x} + \frac{\partial FVD}{\partial y} + \frac{\partial F\omega}{\partial \sigma} = 0, \quad (58)$$

where F is either U , V , T or S . We want the numerical advection technique to be 2nd order accurate in areas with small gradients, gradient preserving near fronts

and monotonic. Among the many recent advection schemes claiming to satisfy these conditions we have chosen to use a superbee limiter scheme due to Roe and Sweby [30]. This scheme performed favorably in a comparison due to Yang and Przekwas [34]. Also for our applications the scheme has proved to maintain the fronts very well. In Figure 2 the surface layer salinity in Skagerrak after running a 4km model 90 days from 15/3-1990 with this scheme is shown.

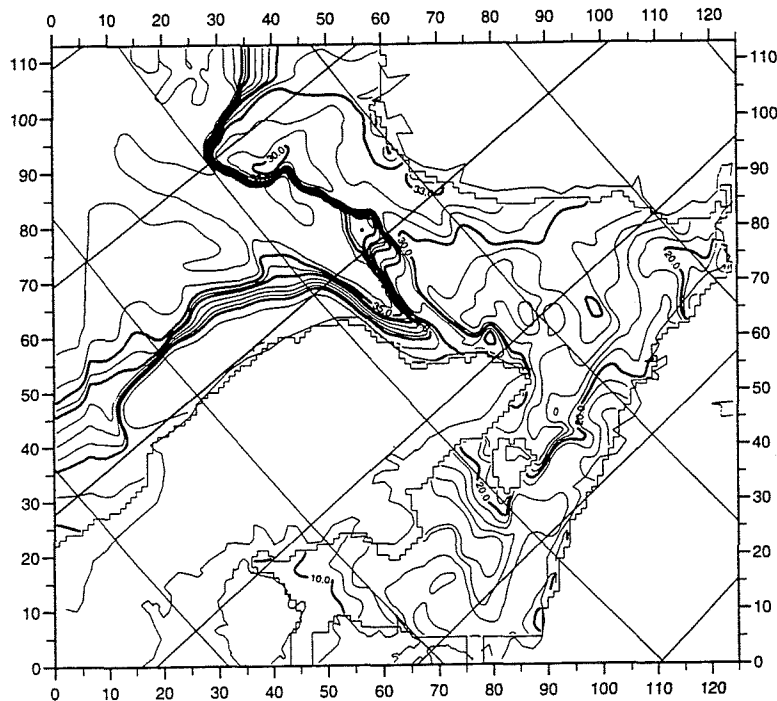


Figure 2. Surface layer salinity in Skagerrak produced by the superbee limiter technique.

For one dimensional problems the algorithm is described in detail in [34]. In our three dimensional implementations the fluxes in all three dimensions are computed before updating the fields on the new time step. The routine for advecting U and V is called SUPERBEEUV. The routine for advection of scalar fields defined in S and T points is called SUPERBEEF.

2.9 Subgrid scale vertical mixing processes

With the present spatial resolution of ocean models many of the important mixing processes will not be resolved. Model results are sensitive to how the effects of these processes are represented and in particular this applies for the vertical mixing processes. A number of choices have been implemented in different models, but to

pick an algorithm that generally is superior to the competitors seems impossible.

In equations (23), (24), (25) and (26) the effects of the vertical subgrid scale processes are represented by terms on the form

$$\frac{\partial}{\partial \sigma} \left(\frac{K}{D} \frac{\partial F}{\partial \sigma} \right),$$

but it is not obvious that this is the best way of including the effects of these processes.

We have experimented with different techniques. Some of these, and the arguments for the choices in the present version of the model, are presented below. Our experience is mainly from the North Sea and Skagerrak. In certain periods the vertical salinity structure of the water masses leaving Skagerrak along the Norwegian coast is known. If this structure is reproduced by the model, it will be a good indication that the effects of the mixing processes are well represented. We have used the Mellor and Yamada [16] 2 1/2 level model with and without the modifications due to Galperin et al. [9]. We often find, for both alternatives, that $K_H \sim K_M$ and that the surface water masses in Skagerrak becomes too saline. In the summer the near surface salinity may be less than 30 p.s.u. in large parts of Skagerrak, see [7, 8]. We do not get such model water near the surface when using this model to produce both K_H and K_M . An alternative would be to use some simple Richardson number formulation. We have tried the formulation due to Munk and Anderson [18]

$$\begin{aligned} K_H &= A_0(1 + 3.33 Ri)^{-1.5} \\ K_M &= A_0(1 + 10 Ri)^{-0.5} \end{aligned}$$

where A_0 is a function of the wind speed and Ri the Richardson number. Also for this formulation we find that the surface layer gets too saline due to too much vertical mixing. The routine RICH computes K_H and K_M according to the above algorithm.

Therefore, a very simple vertical mixing algorithm for scalar fields was tried. The main technique for representing vertical exchange processes of scalar fields is to swap the fields of cells i, j, k and $i, j, k + 1$ whenever $\rho_{ijk} > \rho_{ijk+1}$. This is repeated up to $KB - 1$ times after each update of the temperature and salinity fields. After advecting S and T and updating ρ , the routine STABLE performs these tests and possible exchanges. With the resolution we have in Skagerrak, 4km horizontally and 11 layers in the vertical, we find that with this technique we are able to maintain

a surface layer with salinities similar to those observed during the SKAGEX experiment. How 'close' the model surface fields are to the observed fields depend of course on how the momentum is mixed vertically.

If we apply the Munk and Anderson formulation for K_M , the momentum is typically transferred to deeper layers too quickly and we get very little vertical mixing due to convection. Thus, using this technique for computing K_M , we may find model surface water with salinity less than 10 p.s.u. at the outflow of Skagerrak which is not in accordance with observed values. Therefore, we apply the Mellor and Yamada 2 1/2 level model with the Galperin et al. modifications to compute K_M . The governing equations in z -coordinates for turbulent kinetic energy, $q^2/2$, and turbulent macroscale, l , are given below, see [9, 16],

$$\begin{aligned} \frac{\partial q^2}{\partial t} + \vec{U} \cdot \nabla q^2 + W \frac{\partial q^2}{\partial z} &= \frac{\partial}{\partial z} (K_q \frac{\partial q^2}{\partial z}) + \\ 2K_M \left[\left(\frac{\partial U}{\partial z} \right)^2 + \left(\frac{\partial V}{\partial z} \right)^2 \right] + \frac{2g}{\rho_0} K_H \frac{\partial \rho}{\partial z} - \frac{2q^3}{B_1 l} & \end{aligned} \quad (59)$$

$$\begin{aligned} \frac{\partial q^2 l}{\partial t} + \vec{U} \cdot \nabla q^2 l + W \frac{\partial q^2 l}{\partial z} &= \frac{\partial}{\partial z} (K_q \frac{\partial q^2 l}{\partial z}) + \\ l E_1 K_M \left[\left(\frac{\partial U}{\partial z} \right)^2 + \left(\frac{\partial V}{\partial z} \right)^2 \right] + \frac{l E_1 g}{\rho_0} K_H \frac{\partial \rho}{\partial z} - \frac{q^3}{B_1} \tilde{W} & \end{aligned} \quad (60)$$

where

$$\tilde{W} = 1 + E_2 \left(\frac{l}{\kappa L} \right)^2 \quad (61)$$

and where

$$L^{-1} = (\eta - z)^{-1} + (H + z)^{-1}. \quad (62)$$

$\kappa = 0.4$ is the von Karman constant. Defining

$$G_H = \frac{l^2}{q^2} \frac{g}{\rho_0} \frac{\partial \rho}{\partial z} \quad (63)$$

the stability functions become

$$S_H[1 - (3A_2B_2 + 18A_1A_2)G_H] = A_2[1 - 6A_1/B_1] \quad (64)$$

and

$$S_M[1 - 9A_1A_2G_H] - S_H[18A_1^2 + 9A_1A_2)G_H] = A_1[1 - 3C_1 - 6A_1/B_1] \quad (65)$$

K_M and K_q are then computed according to

$$K_M = lqS_M \quad (66)$$

$$K_q = 0.20lq \quad (67)$$

The empirical values in the expressions above are

$$(A_1, A_2, B_1, B_2, C_1, E_1, E_2) = (0.92, 0.74, 16.6, 10.1, 0.08, 1.8, 1.33) \quad (68)$$

At the surface the following boundary conditions are used

$$q^2 = B_1^{2/3}u_{\tau_s} \quad (69)$$

$$l = 0.0246u_{10}^2 \quad (70)$$

where $u_{\tau_s} = (\overline{\tau}_0^2)^{1/2}$ and $0.0246u_{10}^2$ is an approximation to the surface wave height as a function of the wind speed, u_{10} , 10m above the water surface, see [10]. This is a modification of the original Mellor-Yamada model where $l = 0$ at the surface. In ocean models this is not, as commented by others for instance Blumberg and Mellor [6], a realistic surface boundary condition. With the present formulation we are able to maintain a surface layer in Skagerrak with salinities in more agreement with observed values. With the zero condition, we tend to get too much energy in the surface layers, much vertical convection and a too saline surface layer.

The routine UPSTREAMQ advects the fields q^2 and q^2l with the simple upstream method. Computation of the remaining terms of equations (59) and (60) and the computations of G_M , G_H , S_M , S_H , K_M and K_q are performed in the routine MY2HALV.

2.10 Subgrid scale horizontal mixing processes

Terms of the type (9), (10) and (11) are often included in ocean models to include the effects of subgrid scale horizontal mixing processes. In many cases it is also

necessary to include such terms with large enough values of A_M and/or A_H to avoid instabilities.

With the present choice of advection scheme, see Section 2.8, overshooting/undershooting near fronts is avoided and we may run this model without including horizontal eddy viscosity/diffusivity terms. Also the fractional step method for advecting the surface gravity waves will damp the short scale 2-D modes.

We want to preserve the fronts of the scalar fields as well as possible and we have chosen to use $C_H = 0$ (and thus $A_H = 0$) in our model. Small non-zero values have been tried, but as we increase A_H the quality of the model results for Skagerrak tend to degrade slowly. So our findings is that $A_H = 0$ is the best and also computationally simplest choice.

The fronts in our model density fields may be very sharp and therefore $C_M = 0$ (and $A_M = 0$) will cause strong advective/convective processes near the fronts. The model results for the North Sea and Skagerrak are not very sensitive to the choice of C_M , but the choice $C_M = 0.5$ seems to produce model fields in reasonable agreement with observed fields. A_M is computed according to (12) in the routine SMAGOR. The viscosity fluxes due to the terms DF_x and DF_y of equations (23) and (24) are computed in the advection routine SUPERBEEUV and added to the advective fluxes before updating U and V at the new time step.

2.11 Time step constraints

There are no time step constraints for the inertia-gravity modes because they are transported with implicit techniques.

The internal waves are propagated with an explicit technique and the CFL criterion is $\Delta t < \frac{\Delta x}{c_i}$ where c_i is the maximum internal gravity wave speed in the model area. c_i depends on the stability of the model water masses which develop dynamically, and for small values of Δx and large values of Δt which we want to apply, numerical instabilities may occur because this criterion is violated.

For the advection steps the time step criterions become

$$\Delta t < \text{MIN} \left(\frac{\Delta x}{U}, \frac{\Delta y}{V}, \frac{\Delta z}{\omega} \right). \quad (71)$$

When using thin layers near the surface ($\Delta z < 1$), which we often have in shallow areas, this criterion may be violated because Δt becomes larger than $\frac{\Delta z}{\omega}$.

3 Model validation

3.1 Model validation using SKAGEX-90 data

During SKAGEX-90 [7] fixed hydrographical stations along 8 sections were taken every third day in the period from 24 May to 20 June 1990, see Figure 3. From this dataset temporal mean values and standard deviations of salinity and temperature are produced and compared to corresponding statistics produced from model results produced by the Blumberg and Mellor model, see [5], and the present model. Both models are implemented over a 4km model area, see Figure 2, and we are using 11 layers in the vertical. Initial and boundary values are produced by 20km resolution North Sea models.

Here we will focus on data from section H at the inflow/outflow of Skagerrak, see Figure 3. Average values of salinities produced from observed values are given in Figure 4. Average model results produced by the Blumberg and Mellor model with parameter settings as in the public domain version are presented in Figure 5, and corresponding model results for the present model are given in Figure 6.

In order to quantify the discrepancies between model results and observed values, the following error measure is suggested, see [5]

$$D_{\bar{S}} = (\bar{S}_{model} - \bar{S}_{data})/S_{SD-data}$$

where \bar{S}_{model} is the average modelled salinity, \bar{S}_{data} the average measured salinity and $S_{SD-data}$ the standard deviation in the salinity data. Also area averages of the absolute values of this error measure are computed. In Table 1 these error measures are reported.

Based on both the sectional modelled and measured density fields we have used the thermal wind relation

$$-f \frac{\partial v}{\partial z} = \frac{g}{\rho_0} \frac{\partial \rho}{\partial x}$$

to estimate the velocities normal to the sections. ρ is the model result or data density computed from salinity and temperature using the equation of state. We have assumed zero velocity at the bottom. The barotropic current component is not known from data and therefore this will not give the correct picture of the actual flow through the sections, but in this context the differences in model and data geostrophic currents and transports are of greatest interest. For all velocity fields total transports in and out of the sections are computed. The transports measured in Sverdrups ($1\text{Sv} = 10^6\text{m}^3\text{s}^{-1}$) are given in Table 1. Based on average values of

model velocities for the Skagex period transports are computed and given in Table 1.

Measure	Data	B & M	Present model
$D_{\bar{S}-aver}$	*	5.74	1.80
Model transport-out	*	1.779	0.663
Model transport-in	*	1.750	0.665
Geostrophic transport-out	0.639	3.238	1.268
Geostrophic transport-in	0.255	0.087	0.131

Table 1. Measures transect H.

With the present resolution the internal Rossby radius in Skagerrak is not well resolved so it may be argued that we can not trust model results produced by any model with the present resolution. However, in the foreseeable future the problem with important unresolved processes will be present in most model studies and it is hoped that with a reasonable representation of subgrid scale processes, we may get at least a good picture of the general circulation. Anyway, the capacity of the available computers will always limit the resolution and we should try as best we can with the resolution we can afford.

Some may argue that we now have reached a state where the quality of the ocean models is good enough and that the focus in future should be on applications. The experience from the MOMOP [20] validation was that ocean models could produce quite different results even on simple test cases. In the present Skagerrak study we note that even for similar codes, both σ -coordinate and with the same spatial resolution, the plots of figures 5 and 6 and the numbers of Table 1 are remarkably different. We find that the model transports differ with almost a factor 3.

Both models produce circulation patterns in agreement with what is believed to be the general circulation in Skagerrak, and many of the major processes, that can be represented with the present resolution, are reproduced by both models. See [29] for further results produced by the Blumberg and Mellor model. The numbers above show that even if the models reproduce known circulation patterns qualitatively reasonably well, the transports computed by the models may be very uncertain.

We do not claim that the present model generally is superior to the Blumberg and Mellor model. The results are sensitive to the parameter setting, see [5]. However, we believe that for model areas like Skagerrak and Kattegat with strong density

gradients it is important to apply non-oscillatory advection schemes to avoid under- and over shooting near the fronts. When using the leapfrog scheme for advection, as in the Blumberg and Mellor model, we tend to get too much vertical mixing and the internal pressure gradients at the outflow of Skagerrak become too strong, see figures 4 and 5 and Table 1.

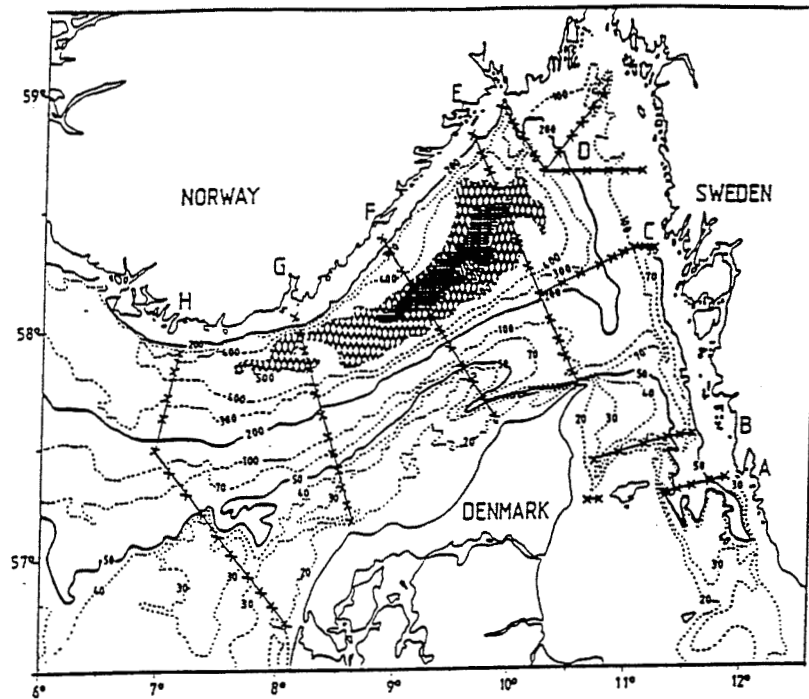


Figure 3. Topography of Skagerrak. A, B, C, D, E, F, G and H show the different sections with the positions of the hydrographical stations. Areas deeper than 500m are hatched and the 50 and 200m bottom contours are enhanced. (From Danielssen *et al.*, 1995)

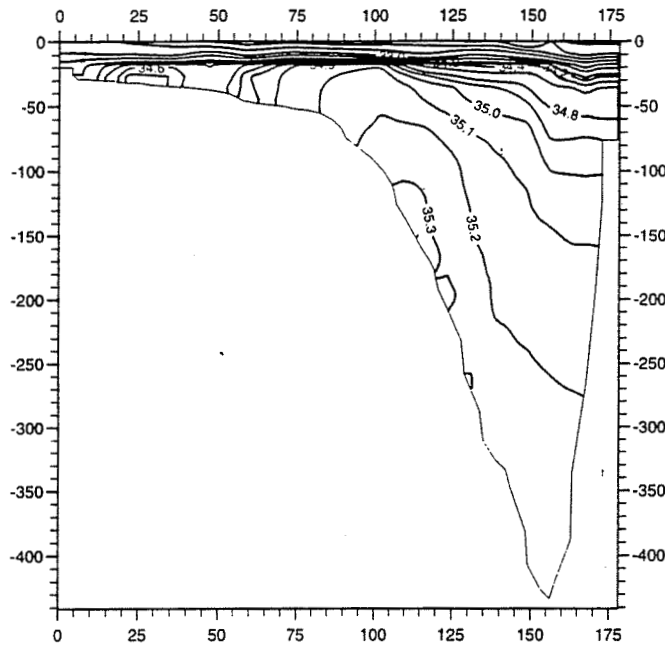


Figure 4. Mean values of observed salinity for section H.

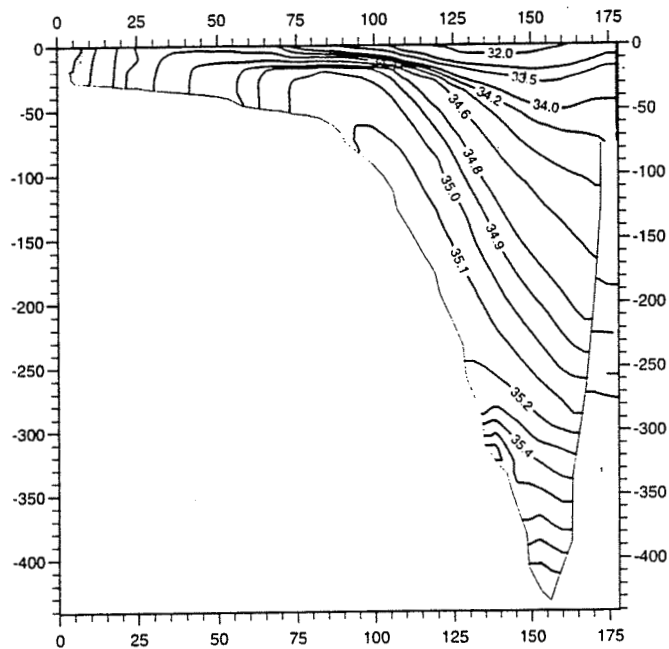


Figure 5. Model mean salinity for section H produced by the Blumberg and Mellor model.

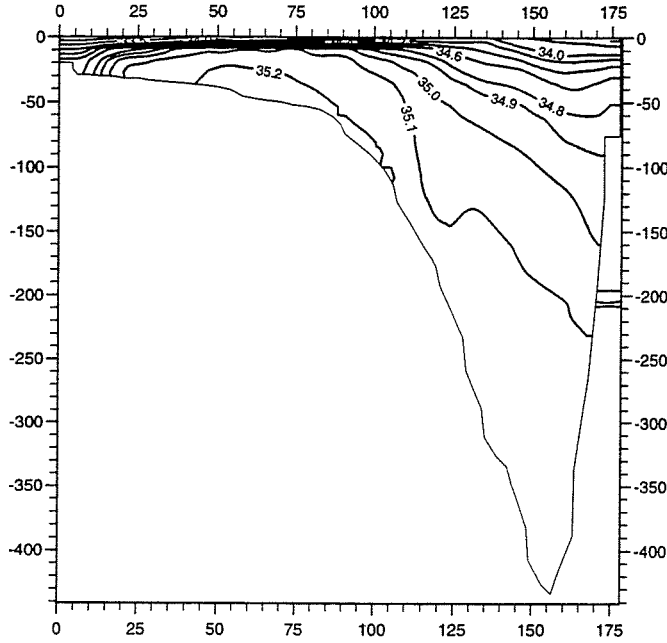


Figure 6. Model mean salinity for section H produced by the present model.

3.2 Validation using an idealized test case

The model is implemented on an idealized test case for two reasons

1. To study whether model results are in agreement with general theory and earlier numerical experiments.
2. To make the implementation of the model on this test case available to other users.

The problem, flow over seamounts in a stratified ocean, is described in detail by Slørdal *et al.* [25]. The model domain is $0 \leq x \leq L_x$, $0 \leq y \leq L_y$ with $L_x = 70000m$ and $L_y = 200000m$. There are vertical walls at $x = 0$ and $x = L_x$, and open boundaries at $y = 0$ and $y = L_y$. A bell shaped seamount centered at the point $(x_c, y_c) = (L_x/2, 50000m)$ grows in time according to

$$H(x, y, t) = H_0 - \delta(t)\Delta H e^{-(r/R)^2}$$

with $r^2 = (x - x_c)^2 + (y - y_c)^2$, H is the model depth, $H_0 = 250m$, $\Delta H = 150m$, $R = 10000m$. The growth function $\delta(t)$ is given by $\delta(t) = 1 - e^{-1.3 \times 10^{-5}t}$. Above

a depth, $h_1(x)$, the density is initially $\rho_0 = 1025 \text{kgm}^{-3}$. Below a depth, $h_2(x)$, the density is initially $\rho_b = 1027.5 \text{kgm}^{-3}$. Between the two depths the density varies linearly. The depths are defined according to

$$\begin{aligned} h_1(x) &= h_{01}(1 + a(x - L_x/2)), \\ h_2(x) &= h_{02}(1 + a(h_{01}/h_{02})(x - L_x/2)), \end{aligned}$$

where $h_{01} = 40 \text{m}$, $h_{02} = 90 \text{m}$, and $a = 2.7 \times 10^{-5} \text{m}^{-1}$. Initially $u = w = 0$, and v and η are computed assuming geostrophic balance, see [25]. Below $h_2(x)$ $v = 0.02 \text{ms}^{-1}$ in our implementation.

The horizontal model resolution is 2.5 km. The interior model domain thus consists of 28×80 grid points. In our implementation we have added one grid cell on each side of the interior model domain in x -direction which are defined as land cells. At the inflow and outflow 10 cell wide FRS-zones, see [12], are added to the interior model domain. In these zones the initial values of all variables are used as external values.

In Figure 7 the 85m depth currents and densities after 72, 144, 192 and 240 hours are shown. The plots of Figure 7 should be compared to FIG. 15 in [25].

The numerical solution of this problem will depend on the choices of parameters. For the results presented in Figure 7 we have used no bottom friction and $\text{CM} = 1.0$. With these choices we get results in qualitative agreement with the results of Slørdal *et al.* [25].

Acknowledgements. We thank the Skagex participants for making the Skagex dataset available for model evaluation and the Norwegian Meteorological Institute for supplying the atmospheric forcing. Comments from Lars Asplin concerning the computations of vertical velocities are appreciated. Thanks to Leiv H. Slørdal for interesting discussions on the internal pressure terms.

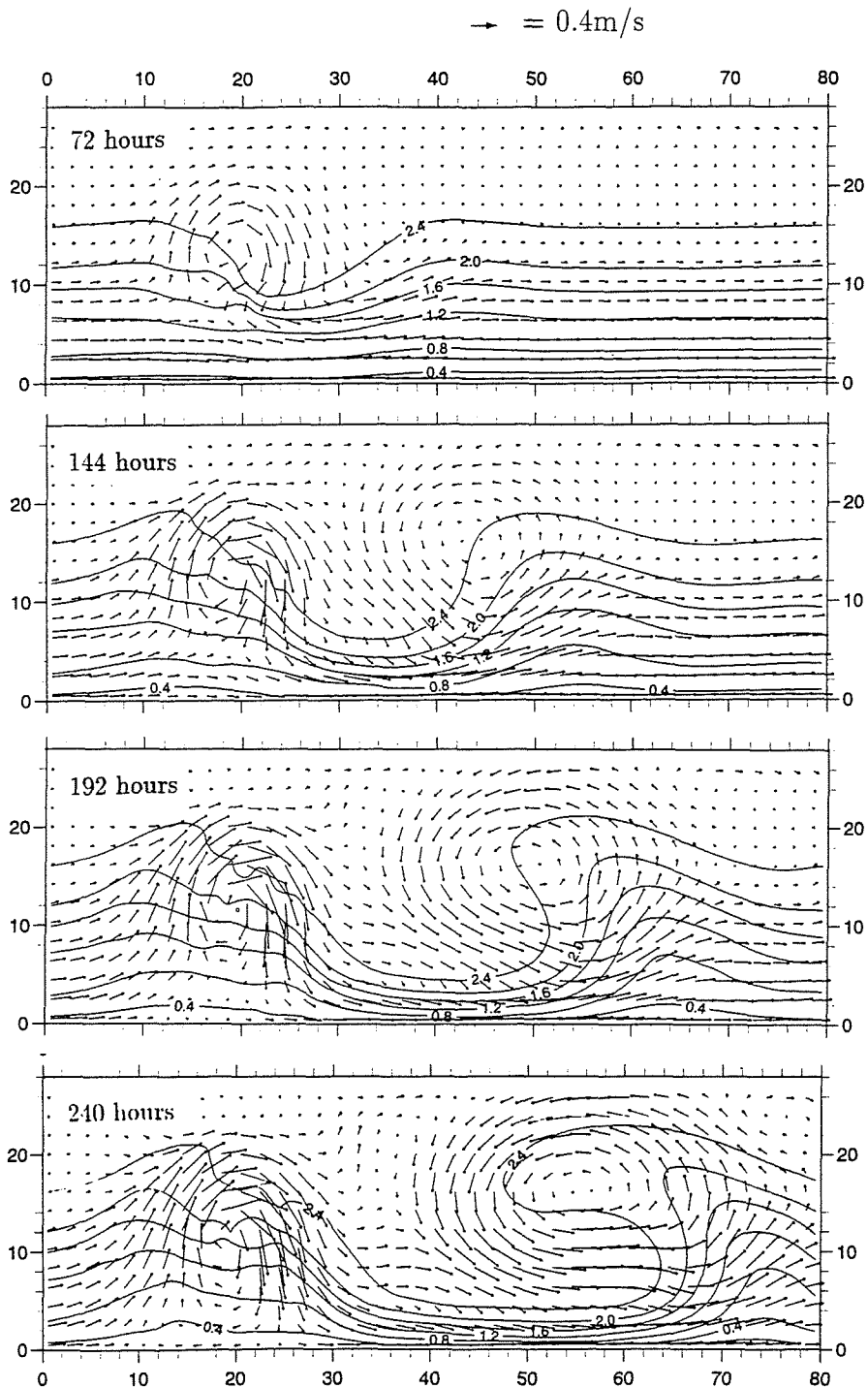


Figure 7. Temporal evolution of 85-m depth currents and density (kg m^{-3}). Every second velocity vector is plotted. The solid lines are isopycnals. For actual density add 1025 kg m^{-3} .

A List of symbols

$\vec{U} = (U, V)$	Horizontal velocities in x - and y -direction respectively
W	Vertical velocity in the z -coordinate system
ω	Vertical velocity in the σ -coordinate system
η	Surface elevation
H	Bottom static depth
D	Bottom dynamic depth ($H + \eta$)
P	Pressure
P_{atm}	Atmospheric pressure
T	Temperature
S	Salinity
ρ	In situ density
K_M	Vertical eddy viscosity
A_M	Horizontal eddy viscosity
C_M	Dimensionless horizontal eddy viscosity coefficient
K_H	Vertical eddy diffusivity
A_H	Horizontal eddy diffusivity
C_H	Dimensionless horizontal eddy diffusivity coefficient
$q^2/2$	Turbulent kinetic energy
l	Turbulent macroscale
ρ_0	Reference density
g	Gravity
f	The Coriolis parameter
$\vec{\tau}_0 = (\tau_{0x}, \tau_{0y})$	Surface wind stress
$\vec{\tau}_b = (\tau_{bx}, \tau_{by})$	Bottom stress
\dot{T}_0	The surface heat flux
\dot{S}_0	The net precipitation/evaporation at the surface
$\vec{U}_b = (U_b, V_b)$	Horizontal velocities at the bottom
W_0	Vertical velocity at the surface (z -coordinate)
W_b	Vertical velocity at the bottom (z -coordinate)
C_D	Bottom drag coefficient
κ	The von Karman constant
z_0	Bottom roughness parameter

B FORTRAN 90 variables

The main variables of the code are defined in MODULE STATE. In the following table a description of the variables is given.

IM	Number of grid cells in x -direction
JM	Number of grid cells in y -direction
KB	Number of grid cell interfaces vertically
DX	The grid spacing in x -direction (m)
DY	The grid spacing in y -direction (m)
DT	The model time step (s)
GRAV	Gravity (ms^{-2})
RHO0	Reference Density
PMEAN	Mean atmospheric pressure
CM	The horizontal viscosity parameter
CD	Minimum value of the bottom drag coefficient
Z0	Bottom roughness parameter

1-D arrays of dimension KB

Z	The σ -coordinates of cell interfaces
ZZ	The σ -coordinates at cell centers ($ZZ(K) = (Z(K)+Z(K+1))/2$)
DZ	Thickness in σ -coordinates of cells ($DZ(K) = Z(K)-Z(K+1)$)
DZZ	Distance in σ -coordinates between cell centers ($DZZ(K) = ZZ(K) - ZZ(K+1)$)
DZR	1/DZ

2-D arrays of dimension (IM,JM)

COR	The Coriolis parameter
ALPHA	$\text{COS}(\text{COR} \cdot \text{DT})$
BETA	$\text{SIN}(\text{COR} \cdot \text{DT})$
FSM	Mask array for cell-centered variables FSM = 0 in land points FSM = 1 in ocean points
DUM	Mask array for variables defined in U-points DUM = 0 in land points DUM = 1 in ocean points
DVM	Mask array for variables defined in V-points DVM = 0 in land points DVM = 1 in ocean points
ETA	The water level
ETAP	The water level at the previous time step
H	Static depth in ETA points
HU	Static depth in U points
HV	Static depth in V points
D	Dynamic depth in ETA points ($D = H + \text{ETA}$)
DU	Dynamic depth in U points
DV	Dynamic depth in V points
WUSURF	Momentum flux in x -direction at the surface
WVSURF	Momentum flux in y -direction at the surface
WUBOT	Momentum flux in x -direction at the bottom
WVBOT	Momentum flux in y -direction at the bottom
WSSURF	Salinity flux at the surface
WTSURF	Heat flux at the surface
PATM	Atmospheric pressure
CBC	Bottom drag coefficients
WSPEED10	Wind speed 10m above sea surface

3-D arrays of dimension (IM, JM, KB)

U	Horizontal velocity in x -direction
V	Horizontal velocity in y -direction
W	σ -coordinate vertical velocity
WR	z -coordinate vertical velocity
UADV	Horizontal velocity in x -direction used for advection
VADV	Horizontal velocity in y -direction used for advection
	The fields UADV, VADV, W and ETA satisfy the equation of continuity
S	Salinity
T	Temperature
RHO	Density
AM	Horizontal viscosity coefficients
KM	Vertical viscosity coefficients
KM	Horizontal viscosity coefficients
Q2	q^2 , turbulent kinetic energy
Q2L	$q^2 l$, turbulent kinetic energy times length scale
DDZ	Dynamic thickness of a cell in a S or T point
DUDZ	Dynamic thickness of a cell in a U point
DVDZ	Dynamic thickness of a cell in a V point

C FORTRAN 90 subroutines

The table below briefly describes the tasks of different subroutines.

CORIOLIS	Effects of earths rotation
SPLITGX	Surface gravity waves in x -direction
SPLITGY	Surface gravity waves in y -direction
CRANK	Surface gravity waves (without dimensional splitting)
GAUSSIT	Iterative solver called from CRANK
INTERNAL	Effects of internal pressure
ZSPL2	Defines quadratic splines in the vertical
SPL2	Evaluates a quadratic spline in the vertical
ATMOSP	Effects of atmospheric pressure
SMAGOR	Computes A_M
SUPERBEEUV	Advection and diffusion of momentum
VERTVISCUV	Vertical mixing of momentum
WREAL	Computes the vertical z -coordinate velocity
SUPERBEEF	Advection of T and S
VERTDIFF	Vertical mixing of T and S
STABLE	Mixes water masses vertically when they are unstable
DENS	The equation of state
UPSTREAMQ	Advection of q^2 and q^2l with the upstream method
MY2HALV	The Mellor-Yamada algorithm for computing K_M and K_H
RICH	A Richardson number based algorithm for computing K_M and K_H
TRIDIA	A tri-diagonal equation solver
MTRIDIA	Solves M tri-diagonal equations
UPDATEDD	Updates Dynamic Depths

References

- [1] D.L. Aksnes, K.B. Ulvestad, B.M. Balino, J. Berntsen, J.K. Egge, and E. Svendsen. Ecological modelling in coastal waters: Towards predictive physical-chemical-biological simulation models. *OPHELIA*, 41:5–36, 1995.
- [2] J. Berntsen and T.O. Espelid. Propagation of shallow water inertia-gravity waves with fractional step methods. Technical Report 100, Department of Applied Mathematics, University of Bergen, Norway, 1995.

- [3] J. Berntsen and T.O. Espelid. On the use of fractional step methods in baroclinic ocean models, 1996. In preparation.
- [4] J. Berntsen, D.W. Skagen, and E. Svendsen. Modelling the transport of particles in the North Sea with reference to sandeel larvae. *Fisheries Oceanography*, 3:81-91, 1994.
- [5] J. Berntsen, E. Svendsen, and M. Ostrowski. Validation and sensitivity study of a sigma-coordinate ocean model using the skagex dataset, 1996. In preparation.
- [6] A.F. Blumberg and G.L. Mellor. A description of a three-dimensional coastal ocean circulation model. In N. Heaps, editor, *Three-Dimensional Coastal Ocean Models, Vol.4*. American Geophysical Union, 1987.
- [7] D.S. Danielssen, L. Davidsson, L. Edler, E. Fogelquist, S. Fonselius, L. Føyn, L. Hernroth, B. Håkansson, I. Olsson, and E. Svendsen. SKAGEX: Some preliminary results. ICES C.M.1991/C:2.
- [8] D.S. Danielssen, L. Edler, S. Fonselius, L. Hernroth, M. Ostrowski, E. Svendsen, and L. Talsepp. Oceanographic variability in Skagerrak/Kattegat may-june 1990, 1992. unpublished.
- [9] B. Galperin, L.H. Kantha, S. Hassid, and A. Rosati. A quasi-equilibrium turbulent energy model for geophysical flows. *J. Atmos. Sci.*, 45:55-62, 1988.
- [10] SWAMP group. Sea wave modelling project (SWAMP). An intercomparison study of wind wave predictions models, part 1: Principal results and conclusions, 1985. in *Ocean Wave Modelling*, Plenum, New York, 256p.
- [11] R.L. Haney. On the pressure gradient force over steep topography in sigma coordinate ocean models. *J. Phys. Oceanogr.*, 21:610-619, 1991.
- [12] E.A. Martinsen and H. Engedahl. Implementation and testing of a lateral boundary scheme as an open boundary condition in a barotropic ocean model. *Coastal Engineering*, 11:603-627, 1987.
- [13] E.A. Martinsen, H. Engedahl, G. Ottersen, B. Ådlandsvik, H. Loeng, and B. Balino. Climatological and hydrographical data for hindcast of ocean currents. Technical Report Tech. Rep 100, The Norwegian Meteorological Institute, 1992.
- [14] G.L. Mellor and A.F. Blumberg. Modelling vertical and horizontal diffusivities in the sigma coordinate system. *Mon. Weather Rev.*, 113:1379-1383, 1985.

- [15] G.L. Mellor, T. Ezer, and L.-Y. Oey. The pressure gradient conundrum of sigma coordinate ocean models. *J. Atmos. Oceanic Technol.*, 11:1126–1134, 1994.
- [16] G.L. Mellor and T. Yamada. Development of a turbulence closure model for geophysical fluid problems. *Rev. Geophys. Space Phys.*, 20:851–875, 1982.
- [17] F. Mesinger and A. Arakawa. Numerical methods used in atmospheric models, volume i, 1976. Garp Publication Series No. 17.
- [18] W.H. Munk and E.R. Anderson. Notes on a theory of the thermocline. *J. Marine Res.*, 7:276–295, 1948.
- [19] N.A. Phillips. A coordinate system having some special advantages for numerical forecasting. *J. of Meteorology*, 14:184–185, 1957.
- [20] L.P. Røed, B. Hackett, and H. Skåtun. Metocean modeling project (MOMOP): Final report: Results of the model intercomparison (abridged version). Technical Report 89-3312, VERITEC, 1989.
- [21] M.D. Skogen. A user's Guide to NORWECOM. The NORWegian ECOlogical Model system. Technical Report 6, Institute of Marine Research, 1993.
- [22] M.D. Skogen, E. Svendsen, J. Berntsen, D. Aksnes, and K. Ulvestad. Modelling the Primary Production in the North Sea using a coupled Three-dimensional Physical- Chemical-Biological Ocean Model. *Estuarine, Coastal and Shelf Science*, 41:545–565, 1995.
- [23] M.D. Skogen, E. Svendsen, and M. Ostrowski. Quantifying volume and nutrient transports and primary production with the Norwegian Ecological Model System (NORWECOM), 1995. Submitted.
- [24] L.H. Slørdal. *A Numerical Study of Dynamic Processes in a Stratified Ocean of Variable Depth. Part III: The Pressure Gradient Force in Sigma-Coordinate Ocean Models*. PhD thesis, Department of Geophysics, University of Oslo, P.O.Box 1022 Blindern, N-0315 Oslo, Norway, 1995.
- [25] L.H. Slørdal, E.A. Martinsen, and A.F. Blumberg. Modeling the response of an idealized coastal ocean to a traveling storm and to flow over bottom topography. *J. Phys. Oceanogr.*, 24:1689–1705, 1994.
- [26] J. Smagorinsky. General circulation experiments with the primitive equations, I. The basic experiment. *Mon. Weather Rev.*, 91:99–164, 1963.
- [27] G.S. Stelling and J.A.T.M. Van Kester. On the approximation of horizontal gradients in sigma coordinates for bathymetry with steep bottom slopes. *Int.J.Numer.Meth.Fluids*, 18:915–935, 1994.

- [28] G.S. Stelling, A.K. Wiersma, and J.B.T.M. Willemse. Practical aspects of accurate tidal computations. *J. Hydraulic Engineering*, 112:802–813?, 1986.
- [29] E. Svendsen, J. Berntsen, M. Skogen, B. Ådlandsvik, and E. Martinsen. Model simulation of the skagerrak circulation and hydrography during skagex, 1996. Accepted by Journal of Marine Systems.
- [30] P.K. Sweby. High resolution schemes using flux limiters for hyperbolic conservation laws. *SIAM J. Numer. Anal.*, 21:995–1011, 1984.
- [31] D.-P. Wang. Mutual intrusion of a gravity current and density front formation. *J. Phys. Oceanogr.*, 14:1191–1199, 1984.
- [32] T.J. Weare. Errors arising from irregular boundaries in ADI solutions of the shallow-water equations. *Int. J. Numer. Meth. Eng.*, 14:921–931, 1979.
- [33] G. Weatherly and P.J. Martin. On the structure and dynamics of the ocean bottom boundary. *J. Phys. Oceanogr.*, 8:557–570, 1978.
- [34] H.Q. Yang and A.J. Przekwas. A comparative study of advanced shock-capturing schemes applied to burgers equation. *J. Comp. Phys.*, 102:139–159, 1992.